2024 IEEE/RSJ International Conference on Intelligent Robots and Systems (IROS)
October 14-18, 2024. Abu Dhabi, UAE

TacLink-Integrated Robot Arm toward Safe Human-Robot Interaction

Quan Khanh Luu[1], Alessandro Albini[2], Perla Maiolino[2], and Van Anh Ho[1,3*]

***Abstract*— Recent developments in vision-based tactile sensing offer a simple means to enable robots to perceive touch interactions. However, existing sensors are primarily designed for small-scale applications like robotic hands, lacking research on their integration for large-sized robot bodies that can be leveraged for safe human-robot interactions. This paper explores the utilization of the previously-developed vision-based tactile sensing link (called *TacLink*) with *soft* skin as a safety control mechanism, which can serve as an alternative to conventional rigid robot links and impact observers. We characterize the behavior of a robot integrated with the soft *TacLink* in response to collisions, particularly employing a reactive control strategy. The controller is primarily driven by tactile force information acquired from the soft TacLink sensor through a data-driven sim2real learning method. Compared with a standard rigid link, the results obtained from collision experiments also confirm the advantages of our "soft" solution in impact resilience and in facilitating controls that are difficult to achieve with a stiff robot body. This study can act as a benchmark for assessing the efficiency of soft tactile-sensitive skins in reactive collision responses and open new safety standards for soft skin-based collaborative robots in human-robot interaction scenarios.**

I. Introduction

Nowadays, an increasing need exists for robots capable of operating in close proximity to humans and engaging in physical interactions with them. These robots are envisioned as versatile assistants across a wide array of sectors, including both industrial and service-oriented domains. To align with these emerging requirements, the integration of advanced safety mechanisms is deemed essential. Toward this goal, effort has been made to enhance robot structures, frequently entailing the optimization of weight or the integration of supplementary flexible or soft elements. In conjunction with these structural improvements, substantial attention has been devoted to safety enhancements through inherent sensing capabilities, such as 6D force/torque sensors or joint torque sensors. [1]–[3]. Based on these devices, control frameworks devised for safety purposes (such as reflex control, impedance relaxation, and so on) have been developed, which often involve intricate dynamics formulation [4], [5]. Also, a comprehensive collision event pipeline, built upon these foundational studies, was thoroughly discussed in [6]. While these seminal works have made significant long-term contributions to advanced safety features of standard *rigid* robot arms, recent advancements in *soft* tactile skins offer potential alternatives for safety control, given their inherent capacity to eliminate physical impacts [7].

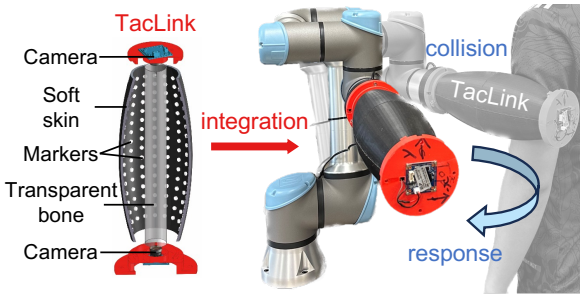

Fig. 1. Research problem: the investigation of safety control for a *soft*, deformable tactile link toward ultimate safe human-robot interaction.

A. Large-scale Soft Tactile Skins

With this respect, *soft* robot skins with tactile sensing capability have recently emerged as an effective solution for physical contact sensation and recognition [8]–[12]. Among various sensor design approaches, tactile (electronic) skins have gained traction due to their scalability and compatibility with existing robotic systems [13], [14]. These skins consist of networks of functional sensing elements, often covered with an external layer made of fabric or elastomer to enhance softness and durability against physical contacts [15]–[18]. Vision-based tactile sensing, on the other hand, has recently enabled tactile perception through intrinsic deformation of soft skin [19]–[22]. Notably, the *TacLink*, a large-scale soft vision-based tactile link, was first introduced in [23], [24] and developed for multimodal sensing [25]. It has demonstrated its ability to effectively convey tactile information, such as contact depth and location, across a whole-arm sensing area through tactile images capturing markers' displacement.

B. Soft Tactile Skins for Collision Handling

In the context of utilizing soft tactile skins to handle unexpected collisions, the mutual effect of a passive soft layer and active collision detection of an electronic tactile skin on eliminating impact forces has been thoroughly investigated [26], in which the soft layer may influence the performance of the active sensing components underneath. While this interference is not expressed in the vision-based soft tactile *TacLink*, which identifies contacts directly from soft skin

This work was supported by JST Precursory Research for Embryonic Science and Technology PRESTO under Grant JPMJPR2038, and SestoSenso (HORIZON EUROPE Research and Innovation Actions under GA number 101070310)

[1]Japan Advanced Institute of Science and Technology (JAIST), Ishikawa, Japan {quan-luu, van-ho}@jaist.ac.jp
[2]Oxford Robotics Institute, University of Oxford, Oxford, England alessandro@robots.ox.ac.uk, perla.maiolino@eng.ox.ac.uk
[3]Japan Science and Technology Agency (JST), PRESTO, Kawaguchi Saitama 332-0012 Japan.
*Corresponding author. Email: van-ho@jaist.ac.jp

deformation; the high compliance and challenging-to-model deformation-force relationship inherent in the large-scale soft contact sensing could impact collision detection and reaction in robotic systems integrated with such sensing device. Characterizing the effectiveness of the soft *TacLink* in reacting to unexpected collisions, especially with reactive control, can potentially advance safety and efficiency in human-robot interaction scenarios. Thus, based on the developed *TacLink* [24] platform, this paper attempts to make the following contributions:

- Investigating the performance of the *TacLink* in facilitating reactive actions towards collisions, characterized by response time and peak impact force. This involves integrating the soft contact sensing capabilities of the *TacLink* with a reactive controller. The outcomes can serve as a benchmark for evaluating the effectiveness of soft tactile-sensitive skins in collision-handling tasks.
- Conducting a comparative study to demonstrate how the softness of the *TacLink* influences reactive control and other collision responses, compared to those observed with a conventional *stiff* robot link. The findings are expected to contribute to the development of new safety standards for soft skin-based collaborative robots in human-robot interaction settings.

Note that this paper primarily focuses on investigating the efficiency of a soft tactile link in collision responses, with the *TacLink* integrated as an extended sensorized link for a commercial robot arm. Thus, our investigation is limited to scenarios where contacts occur on the extended link.

II. Preliminaries of Vision-based Tactile Link

This section briefly outlines the design of the soft vision-based *TacLink* and a sim2real learning approach used to extract necessary contact information for integration into the reactive control system.

A. Sensor hardware

This paper employs a barrel-shaped *soft* vision-based tactile link (*TacLink*), as shown in Fig. 1. The tactile skin sensor with arrays of inner markers (molded from Ecoflex 00–30, Smooth On, USA) is a 360° barrel-shaped body with a camera affixed at each end. Thus, given that the white markers are distributed evenly on the inner skin surface, the *TacLink* can deduce tactile sensory information relying on cues of markers' displacements. While there existed other design structures for the sensor, we have chosen this barrel shape for implementation in this paper due to its high potential for generalization to other robot bodies. Also, this choice allows us to maintain simplicity that resembles standard robot links.

B. Tactile sensing scheme

In order to recognize the tactile stimulus exerted on the whole-arm deformable skin, we utilize a simulation-to-real *sim2real* learning framework, as recently introduced in [24]. Specifically, a Deep Neural Network (DNN) is employed to enable the estimation of skin deformation through the inputs

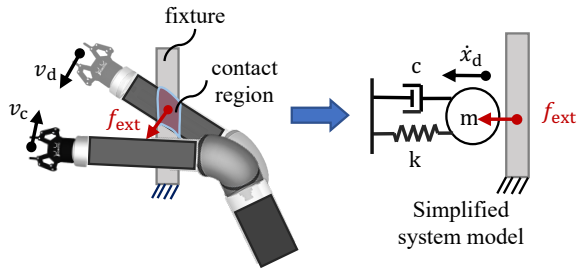

(a) Conceptual implementation of the collision reactive control

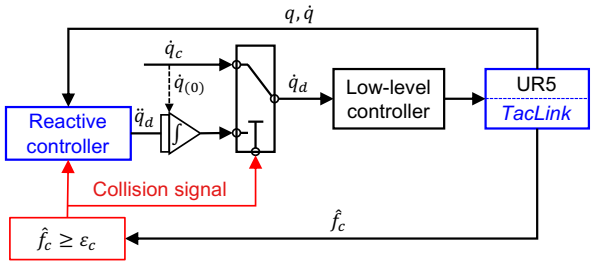

(b) Block diagram of the collision reactive controller

Fig. 2. A kinematics control scheme allowing a robot with tactile sensing link to respond to a physical impact safely.

of tactile images capturing the markers' displacements. The initial RGB input images are initially converted to binary format to facilitate the sim2real learning process while maintaining accuracy. Given that the soft skin is represented by finite element mesh, the DNN estimates the global skin deformation by estimating the 3D displacements of each node on the entire skin surface, which is denoted as $\hat{\mathbf{D}} = [\hat{\mathbf{d}}_i^\top] \in \mathbb{R}^{N\times 3}$ (N indicates the number of mesh nodes). Here, the displacement vector $\hat{\mathbf{d}}_i$ is defined as

$$\hat{\mathbf{d}}_i := \mathbf{x}_i - \mathbf{x}_i^o, \tag{1}$$

where $\mathbf{x}_i \in \mathbb{R}^3$ denotes the 3D position vector of a mesh node, and $\mathbf{x}_i^o \in \mathbb{R}^3$ represents the position of the respective node in its original. Further details about the data collection and training of the DNN can be found in [24]. Consequently, the DNN-predicted global skin deformation enables the estimation of local contact depth as:

$$\hat{d}_c = \max\|\hat{\mathbf{d}}_i\|. \tag{2}$$

In this paper, we assume that only one contact occurs at a time and in the normal direction to the skin surface. The contact intensity is quantified by the contact depth $\hat{d}_c$, which is then mapped to an equivalent contact force (see Eq. 5). This enables the detection of contact, which in turn triggers the reactive controller and collision responses.

III. Collision Reactive Control

This section outlines the integration of the *TacLink* with a kinematics-based reactive control strategy, which highlights how the feedback on contact depth obtained from the *TacLink* is incorporated into the reactive controller.

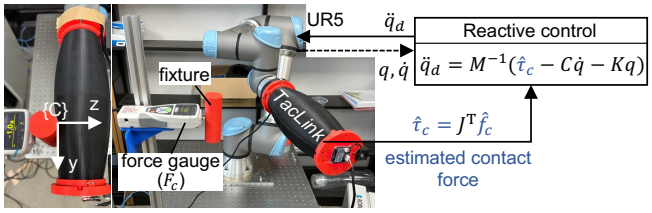

Fig. 3. System integration of the vision-based tactile link and UR5e robot arm and setup schemes for the sensing and collision experiments.

A. Control strategy

To demonstrate the utilization of the tactile sensing link for safety purposes, we attempt to derive a control formulation to address the problem in which a TacLink-equipped robot unexpectedly hits an obstacle at a constant impact velocity, as depicted in Fig. 2. In this paper, we limit the maximum linear velocity of the robot at the contact point to $0.2\,\mathrm{m/s}$ which approximates an allowed velocity set by ISO/TS 15066 standard [27] that guarantees safe human-robot collaborative operations in the Power and Force Limiting setting. To tackle this problem, we employ a reactive controller such that the contact force caused by the impact is as small as not to exceed human biomechanical limits [5], while reversing the robot's velocity direction to move away from the collision area.

In order to satisfy the control objectives, we employ a kinematics admittance controller [4] that treats the robot system as a mass-spring-damper system (see Fig. 2a) with virtual inertia, damping, and stiffness components. Specifically, this reactive controller attempts to accelerate the robot such that the system responds purposefully to the contact force measured by the TacLink sensor. Thus, considering a 6-DOF (degree-of-freedom) robot arm with joint positions $\mathbf{q} \in \mathbb{R}^6$ and joint velocities $\dot{\mathbf{q}} \in \mathbb{R}^6$, the admittance control law can be derived as

$$\ddot{\mathbf{q}}_d = \mathbf{M}^{-1}(\hat{\boldsymbol{\tau}}_c - \mathbf{C}\dot{\mathbf{q}} - \mathbf{K}\mathbf{q}) \tag{3}$$

where $\mathbf{M} \in \mathbb{R}^{6\times6}$ is the positive-definite diagonal virtual inertia matrix, $\mathbf{C} \in \mathbb{R}^{6\times6}$ is the positive-definite diagonal virtual damping matrix, and $\mathbf{K} \in \mathbb{R}^{6\times6}$ is the positive-definite diagonal virtual rotational stiffness matrix. Also, $\hat{\boldsymbol{\tau}}_c$ is the resulting external torque which can be computed as

$$\hat{\boldsymbol{\tau}}_c = \mathbf{J}_c^{\mathrm{T}}\hat{\mathbf{F}}_c \tag{4}$$

where $\mathbf{J}_c \in \mathbb{R}^{6\times6}$ is the Jacobian matrix at the contact point $\mathbf{x}_c \in \mathbb{R}^3$, and $\hat{\mathbf{F}}_c \in \mathbb{R}^6$ is the generalized external contact force with regard to a coordinate system $\{\mathrm{C}\}$ as shown in Fig. 3. The detailed derivation of the contact position $\mathbf{x}_c$ from the nodal displacements $\hat{\mathbf{d}}_i$ can be found in [24]. Note that the admittance control law (Eq. 3) is simplified so that the robot ultimately becomes stationary when no external torque is applied.

B. System integration and implementation

While the described control scheme for handling collisions can be adapted for various tactile sensing skins, our specific implementation focuses on a robot system that extends the end-effector of a standard industrial robot arm with the large-scale tactile sensing link. Due to the fact that the contact depth $\hat{d}_c$ measured by the TacLink sensor (Eq. 2) dominates only in the direction normal to the skin surface, the generalized contact force can be simplified to $\hat{\mathbf{F}}_c = [0,\, 0,\, \hat{f}_c,\, 0,\, 0,\, 0]^{\mathrm{T}}$; where $\hat{f}_c$ is the estimated contact force along the z axis. In addition, the contact depth needs to be mapped to the equivalent contact force $\hat{f}_c$ which is a driving factor of the reactive control law (Eq. 3). While this mapping can be conducted using a high-precision finite element (FE) modeling technique, in this paper, we simplify the calibration procedure by representing the soft skin deformation at a given contact point with an elastic spring element α_f

$$\hat{f}_c = \alpha_f \cdot \hat{d}_c. \tag{5}$$

The calibration procedure for the stiffness constant α_f and the calibrated contact force's accuracy over different regions of TacLink are presented in Section IV-A.

Moreover, this system is characterized by two phases: *before* and *after* a collision (see Fig. 2b). Prior to a collision, the robot is commanded to move with a joint velocity reference $\dot{\mathbf{q}}_c$ possibly generated from a normal motion planner. On the other hand, upon collision, the system immediately switches to the collision reactive controller that triggers the robot's response by the control law $\ddot{\mathbf{q}}_d$ (Eq. 3), which results in reactive joint velocities $\dot{\mathbf{q}}_d$ through time integration. Thus, the overall control system can be formulated as

$$\dot{\mathbf{q}}_d = \begin{cases} \int_{t_0}^{t} \ddot{\mathbf{q}}_d\, dt + \dot{\mathbf{q}}_c(t_0), & \text{if } \hat{f}_c \geq \epsilon_c \\ \dot{\mathbf{q}}_c, & \text{otherwise,} \end{cases} \tag{6}$$

where t_0 indicates the time when the robot gets in contact with an obstacle, which is triggered as the estimated contact force $\hat{f}_c$ is above a constant threshold ϵ_c. The threshold is determined based on the hysteresis characteristic of the TacLink sensor (see Sec. IV-A). Lastly, as a result of Eq. 6, the resulting joint velocity $\dot{\mathbf{q}}_d$ is regulated by the robot's low-level controller. It should be noted that the controllers could have access to the position and velocity joint states $(\mathbf{q},\, \dot{\mathbf{q}})$ through built-in robot joint encoders. The system effectiveness and controller's performance in handling collisions are discussed in Section IV-B.

IV. Experiment

The experimental setup for evaluating the performance of tactile sensing and its integration with a UR5e robot arm for safety control is illustrated in Fig. 3. The system was run on a Ubuntu PC with GPU acceleration to enable high-speed vision-based tactile sensing at approximately $100\,\mathrm{Hz}$. Fig. 4 demonstrates the operation of the TacLink sensing system, where multi-point contacts can be detected based on the input of tactile images. Moreover, the control system was implemented using ROS (robot operating system), specifically utilizing *ros-control* for the low-level velocity control. To interface with the UR5 robot, an official driver package for the UR5 hardware interface was employed.

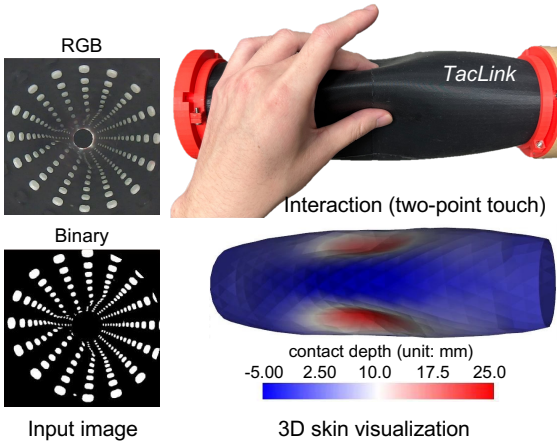

Fig. 4. Visualization of tactile sensing, by which the skin shape under deformation can be constructed from the input image.

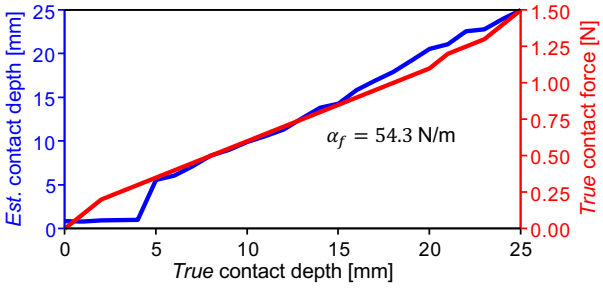

(a) The correlation between contact depth and force

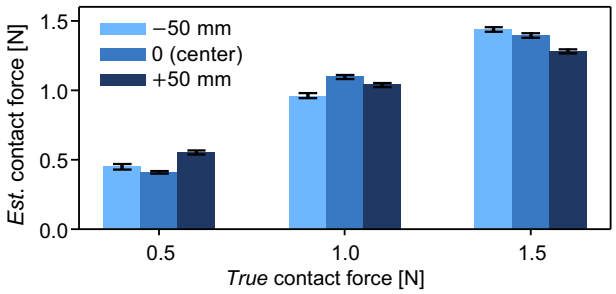

(b) Estimated contact force at different contact regions

Fig. 5. The quantitative evaluation of tactile sensing performance with regard to the contact depth and calibrated contact force.

In the following sections, we first report the accuracy of contact depth sensing and the results of calibrated force measurement, followed by the showcase of the robot's performance in responding to collisions with the assistance of integrated tactile sensing. Lastly, we conduct a study to compare the performance of our proposed soft system against different control strategies applied for collisions occurring on the rigid UR5 forearm link.

A. Tactile sensing system

To assess the accuracy of contact depth sensing and obtain true force values for force calibration, we conducted an experimental setup where the TacLink was pressed against a fixture, attached to a force gauge (Imada, ZTA), along the normal direction to the skin surface (see Fig. 3). We incrementally increased the depth of contact by 1 mm, recording both the estimated contact depth provided by TacLink and the corresponding actual force values. The relationship between the true contact depths and the estimated values, as well as the correlation between the contact depth and measured contact force, are reported in Fig. 5a.

In fact, the contact depth signal exhibited a hysteresis characteristic responsive only to local skin deformations larger than 5 mm, resulting in a minimum contact force recognizable by the TacLink of approximately 0.4 N. Also, the presence of the inner acrylic bone constrained the maximum range of force sensing to around 1.5 N. Based on the observed contact depth-force correlation in Fig. 5a, we derived a quasi-static linear elastic model to represent the relationship between the force and displacement. This model yielded a stiffness constant of $\alpha_f = 54.3\,\mathrm{N/m}$.

Figures 5b report the accuracy of contact depths and calibrated contact forces at three different locations on the TacLink, along its vertical axis: i) at the center region, ii) 50 mm to the left, and iii) 50 mm to the right of the center location. The results showed a consistent sensing pattern among the different contact regions, with the estimated values positively correlated with the true ones. However, there were moderate differences in accuracy between the contact locations. These discrepancies can be attributed to the varying skin stiffness in different regions due to its specific morphology. While we applied a single stiffness constant of a simple linear model to calibrate force values for the entire skin, it may not fully capture the regional variations. Moreover, the maximum deviation of approximately 17 % in contact force between the three regions was observed when the skin experienced a large contact depth of 25 mm. This can be accounted for by the limitations of a linear elastic model in accurately representing large deformations. Nevertheless, considering the observed sensing accuracy and the alignment of measured values with actual ones, the TacLink sensor remains effective for various robotics applications, while leaving room for further improvements.

B. Safety Control System

Settings: This section showcases the capabilities of the *TacLink*-integrated robot in responding to unexpected collisions, employing the reactive control strategy described in Section III. The controller's performance was also evaluated under various control parameters and pre-contact (initial) robot velocities $\dot{\theta}_0$. The experimental scheme is illustrated in Fig. 3, where the TacLink-integrated robot was directed towards a fixture attached to a force gauge at a constant speed $\dot{\theta}_0$. For the sake of simplicity, we focused on the motion of the robot's base joint (*i.e.*, joint 1) and defined the robot configuration, as in Fig. 3, such that the moment arm of the contact force occurring at the fixture is $l_f = 0.5\,\mathrm{m}$ and the matrices of controller parameters can be simplified to $\mathbf{M} = \mathrm{diag}(0.15, [\mathbf{0}]_5^{\mathrm{T}})$, $\mathbf{C} = \mathrm{diag}(c, [\mathbf{0}]_5^{\mathrm{T}})$, and $\mathbf{K}$ is intentionally

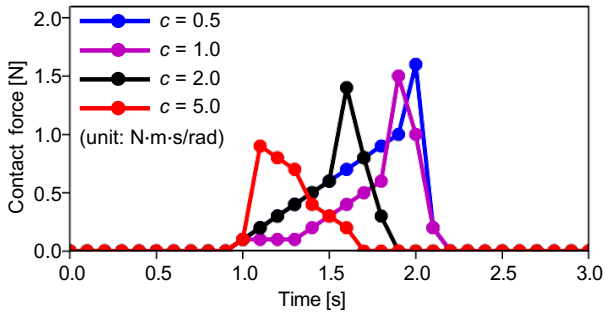

(a) Contact force with the variance of rotational damping coefficient

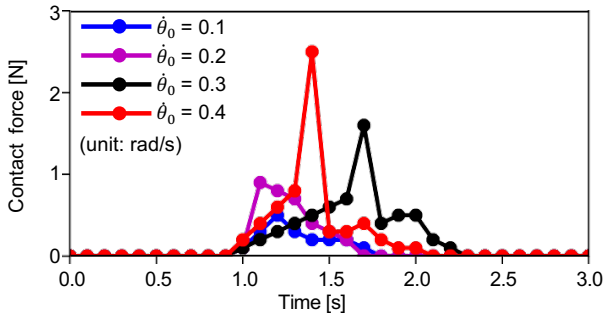

(b) Contact force with the variance of initial (pre-contact) joint speed

Fig. 6. The robot's behavior with different control parameters of the proposed reactive controller.

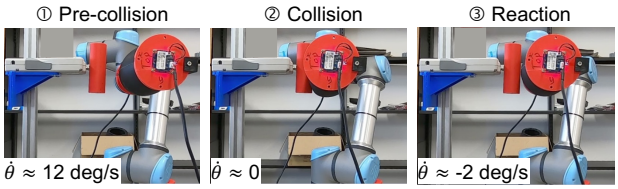

(a) Video stills capturing robot response in collision experiment

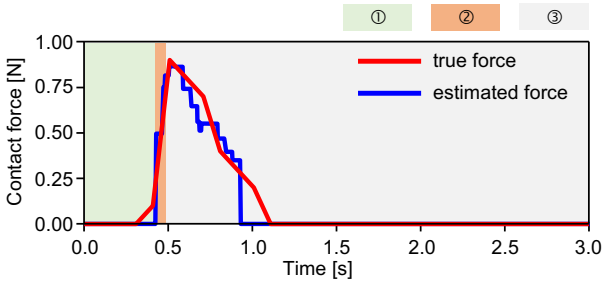

(b) True and estimated contact force during the collision

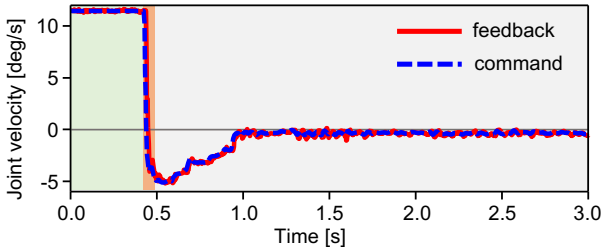

(c) Command joint velocity and its feedback

Fig. 7. The behavior of robot with the application of collision reaction strategy over time.

set to zeros to eliminate the need for specifying a reference position and oscillation behavior. Here, we characterize the soft reactive controller's performance by the *peak impact force* during the collision phase, *recovery duration* from the onset of collision to the time when the contact force is completely diminished, and *reactive duration* measured from the onset of collision to the time when the controller starts reacting, by which smaller values indicate better controller performance.

Results: The examination of how the robot behaves in a collision with various controller parameters is highlighted in Fig. 6. As shown in Fig. 6a, both the peak impact force and recovery duration were reduced with an increase in the rotational damping coefficient c and a constant initial speed of $\dot{\theta}_0 = 0.2$ rad/s. This outcome can be explained by the fact that a larger damping coefficient results in a more significant resistant force opposing the robot's motion toward the collision, thereby alleviating the contact force peak and recovery duration. Fig. 6b displays the robot's responses to collisions with various pre-collision velocities and damping coefficient $c = 5$. Additionally, Fig. 7 exhibits the robot's motion and behavior during three phases: 1) pre-collision, 2) collision, and 3) recovery/reactive phase. The pattern of the estimated contact force closely aligned with actual force values (see Fig. 7b), which verifies the effectiveness of the integrated *soft* sensing system for safety control tasks, even if there was some hysteresis in the sensing signal, particularly for small skin deformation, as reported in Section IV-A. Furthermore, Fig. 7c presents the commanded base joint velocity integrated from the desired joint acceleration $\ddot{q}_d$ computed from the proposed control law. This demonstrates the controller's efforts to move the robot away from the collision region by reversing its moving direction.

Init. speed (rad/s)	*Reactive time* (ms)	*Recovery time* (ms)	*Peak impact force* (N)
$\dot{\theta}_0 = 0.1$	62.0 ± 16.2	820.0 ± 40.0	1.00 ± 0.09
$\dot{\theta}_0 = 0.2$	54.0 ± 29.9	860.0 ± 49.0	1.14 ± 0.16
$\dot{\theta}_0 = 0.3$	72.0 ± 21.4	780.0 ± 40.0	1.42 ± 0.26
$\dot{\theta}_0 = 0.4$	64.8 ± 17.3	640.0 ± 49.0	1.66 ± 0.54

TABLE I

CHARACTERIZATION OF SOFT REACTIVE RESPONSE: RESPONSE TIMES AND PEAK IMPACT FORCE

Table I reports the characterization of the *soft* reactive response for different initial speeds (with $c = 5$). The result highlights the reactive duration, recovery duration, and peak impact force of less than 80 ms, 900 ms, and 2.2 N, respectively, for initial speeds up to 0.4 rad/s (equivalent to an impact linear velocity of 0.2 m/s). The delay in the reactive time can be attributed to the sensitivity of *TacLink*, which varies from one sensor to another. Notably, the observed peak impact forces resulting from collisions with the soft tactile link are well below the threshold considered dangerous for

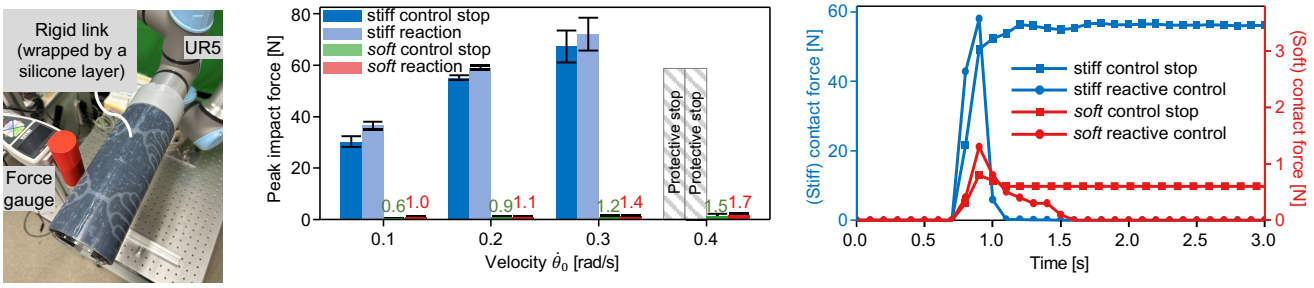

(a) *Stiff* collision setup (b) Comparison of peak impact force (c) Comparison of transient responses ($\dot{\theta}_0 = 0.2$ rad/s)

Fig. 8. Comparison of collision handling performance between a *stiff* and tactile-enabled *soft* link with two different control strategies. The results displayed in (b)-(c) demonstrate the effectiveness of leveraging the soft mechanism with tactile sensing to facilitate reactive control and contact responses. It is observed that the utilization of the soft *TacLink* significantly mitigates peak impact forces. At $\dot{\theta}_0 = 0.4$ rad/s (b), the UR5's built-in controller triggers the *protective stop* signal in the trials of stiff collisions to halt the robot's motion (the observed peak impact forces are not reported for this case).

humans [4], demonstrating the advantages of soft tactile sensing in ensuring safe human-robot interaction. Last but not least, this characterization can act as a benchmark for assessing the efficiency of soft tactile-sensitive skins in handling collisions with reactive control.

C. Comparative Study

Settings: This section verifies the effectiveness of the soft tactile link in mitigating large impact forces compared with a rigid link. The rigid link, constructed from an acrylic pipe, was attached to the UR5's end-effector, similar in size and weight to the soft *TacLink*. Additionally, the rigid link was encased in a silicone rubber pad (see Fig. 8a) to mitigate extreme collision impacts and protect the link from potential damages. For estimating the external contact torque in cases of stiff-link collisions without direct feedback from the tactile sensor, we implemented the $\hat{\tau}$-observer method [4], which relies on simplified joint-space dynamics of the robot base, alongside the inherent joint torque feedback provided by the UR5's low-level controller. Here, we conducted collision experiments to compare the peak impact force and the robot's response resulting from the rigid link and the soft tactile link, employing two collision handling strategies:

1) (Stiff/Soft) Control stop: immediately halts the robot's motion upon contact detection.
2) (Stiff/Soft) Reactive control: described in Section III.

The (stiff/soft) prefix indicates the type of link with which the controller is tested. The collision experiments were performed at various pre-contact velocities, with five trials conducted for each velocity. While the parameter of the reactive controller c was set to 5 in experiments with the soft link, it was experimentally adjusted in the case of the stiff link so that the reaction time matched that observed with the soft counterpart.

Results: Figure 8 summarizes the results obtained from collision responses. As shown in Fig. 8b, collision handling observed on the stiff link experienced much greater peak impact forces, compared to that observed with the soft *TacLink*, regardless of the applied control strategies. Note that, at $\dot{\theta}_0 = 0.4$ rad/s, the UR5's built-in controller activated the *protective stop* signal in response to substantial impact forces detected in the case of stiff link collisions, while the soft link consistently maintained lower impact forces across different velocities (see Fig. 8b). Furthermore, while the stiff reactive control exhibited similar transient responses to its soft counterpart, dissipating contact forces over time (see Fig. 8c), it resulted in significantly higher peak forces compared to the soft reactive control (see Fig. 8c). For instance, shown in Figs. 8b-8c, at $\dot{\theta}_0 = 0.2$ rad/s, the average peak impact force induced by the soft reactive control was approximately 1.1 N, nearly 54 times smaller than that caused by the stiff reactive controller (around 60 N).

The obtained results confirm the effectiveness of utilizing *TacLink* in mitigating peak impact forces, particularly in reactive collision handling scenarios. This finding implies the potential for developing safer robotic arms constructed entirely from soft tactile links.

V. Conclusion and Future Work

The paper demonstrates the effectiveness of employing a vision-based soft tactile link (*TacLink*) to handle unexpected collisions by reducing peak impacts and recovering from contacts, particularly through reactive control. The results indicate that the *TacLink*-integrated robot can quickly move away from the impact region within a duration of approximately 900 ms, while restricting the maximum contact force to below 2.2 N, even with an impact velocity of 0.2 m/s. This level of contact force is well below the dangerous threshold for humans [4]. The comparative study also emphasizes the benefits of the highly-soft sensing skin in eliminating significant impacts caused by collisions and facilitating controls that might be challenging with rigid robot bodies.

In future work, we aim to further investigate the optimal impedance behaviors of the reactive controller across various robot configurations and speeds, guided by a theoretical analysis of system dynamics and control. Additionally, we plan to extend our findings to thoroughly explore new safety standards for soft skin-based collaborative robots, benchmarking our technology against other existing or commercially available large-area tactile robot skins.

REFERENCES

[1] A. De Luca, A. Albu-Schaffer, S. Haddadin, and G. Hirzinger, "Collision detection and safe reaction with the dlr-iii lightweight manipulator arm," in *2006 IEEE/RSJ International Conference on Intelligent Robots and Systems*, 2006, pp. 1623–1630.

[2] A. O. Albu-Schäffer, S. Haddadin, C. Ott, A. Stemmer, T. Wimböck, and G. Hirzinger, "The dlr lightweight robot: design and control concepts for robots in human environments," *Industrial Robot*, vol. 34, pp. 376–385, 2007.

[3] B. Vanderborght, A. Albu-Schaeffer, A. Bicchi, and et al., "Variable impedance actuators: A review," *Robotics and Autonomous Systems*, vol. 61, no. 12, pp. 1601–1614, 2013.

[4] S. Haddadin, A. Albu-Schaffer, A. De Luca, and G. Hirzinger, "Collision detection and reaction: A contribution to safe physical human-robot interaction," in *2008 IEEE/RSJ International Conference on Intelligent Robots and Systems*, 2008, pp. 3356–3363.

[5] S. Haddadin, A. Albu-Schäffer, and G. Hirzinger, "Safety evaluation of physical human-robot interaction via crash-testing." in *Robotics: Science and systems*, vol. 3. Citeseer, 2007, pp. 217–224.

[6] S. Haddadin, A. De Luca, and A. Albu-Schäffer, "Robot collisions: A survey on detection, isolation, and identification," *IEEE Transactions on Robotics*, vol. 33, no. 6, pp. 1292–1312, 2017.

[7] R. S. Dahiya, G. Metta, M. Valle, and G. Sandini, "Tactile sensing—from humans to humanoids," *IEEE Transactions on Robotics*, vol. 26, no. 1, pp. 1–20, 2010.

[8] A. Albini and G. Cannata, "Pressure distribution classification and segmentation of human hands in contact with the robot body," *The International Journal of Robotics Research*, vol. 39, no. 6, pp. 668–687, 2020.

[9] L. Pecyna, S. Dong, and S. Luo, "Visual-tactile multimodality for following deformable linear objects using reinforcement learning," in *2022 IEEE/RSJ International Conference on Intelligent Robots and Systems (IROS)*, 2022, pp. 3987–3994.

[10] A. Albini, F. Grella, P. Maiolino, and G. Cannata, "Exploiting distributed tactile sensors to drive a robot arm through obstacles," *IEEE Robotics and Automation Letters*, vol. 6, no. 3, pp. 4361–4368, 2021.

[11] O. Shorthose, A. Albini, L. He, and P. Maiolino, "Design of a 3d-printed soft robotic hand with integrated distributed tactile sensing," *IEEE Robotics and Automation Letters*, vol. 7, no. 2, pp. 3945–3952, 2022.

[12] R. B. Burns, H. Lee, H. Seifi, R. Faulkner, and K. J. Kuchenbecker, "Endowing a NAO robot with practical social-touch perception," *Frontiers in Robotics and AI*, vol. 9, p. 840335, Apr. 2022.

[13] A. Schmitz, P. Maiolino, M. Maggiali, L. Natale, G. Cannata, and G. Metta, "Methods and technologies for the implementation of large-scale robot tactile sensors," *IEEE Transactions on Robotics*, vol. 27, no. 3, pp. 389–400, 2011.

[14] G. Cheng, E. Dean-Leon, F. Bergner, J. Rogelio Guadarrama Olvera, Q. Leboutet, and P. Mittendorfer, "A comprehensive realization of robot skin: Sensors, sensing, control, and applications," *Proceedings of the IEEE*, vol. 107, no. 10, pp. 2034–2051, 2019.

[15] V. A. Ho, S. Hirai, and K. Naraki, "Fabric interface with proximity and tactile sensation for human-robot interaction," in *2016 IEEE/RSJ International Conference on Intelligent Robots and Systems (IROS)*, 2016, pp. 238–245.

[16] T. P. Tomo, M. Regoli, A. Schmitz, L. Natale, H. Kristanto, S. Somlor, L. Jamone, G. Metta, and S. Sugano, "A new silicone structure for uskin-a soft, distributed, digital 3-axis skin sensor and its integration on the humanoid robot icub," *IEEE Robotics and Automation Letters*, vol. 3, no. 3, pp. 2584–2591, July 2018.

[17] G. Pang, G. Yang, and Z. Pang, "Review of robot skin: A potential enabler for safe collaboration, immersive teleoperation, and affective interaction of future collaborative robots," *IEEE Transactions on Medical Robotics and Bionics*, vol. 3, no. 3, pp. 681–700, 2021.

[18] H. Park, K. Park, S. Mo, and J. Kim, "Deep neural network based electrical impedance tomographic sensing methodology for large-area robotic tactile sensing," *IEEE Transactions on Robotics*, vol. 37, no. 5, pp. 1570–1583, 2021.

[19] A. Yamaguchi and C. G. Atkeson, "Recent progress in tactile sensing and sensors for robotic manipulation: can we turn tactile sensing into vision?" *Advanced Robotics*, vol. 33, no. 14, pp. 661–673, 2019.

[20] W. Yuan, S. Dong, and E. H. Adelson, "Gelsight: High-resolution robot tactile sensors for estimating geometry and force," *Sensors*, vol. 17, no. 12, p. 2762, 2017.

[21] A. Padmanabha, F. Ebert, S. Tian, R. Calandra, C. Finn, and S. Levine, "Omnitact: A multi-directional high-resolution touch sensor," in *2020 IEEE International Conference on Robotics and Automation (ICRA)*. IEEE, 2020, pp. 618–624.

[22] N. F. Lepora, Y. Lin, B. Money-Coomes, and J. Lloyd, "Digitac: A digit-tactip hybrid tactile sensor for comparing low-cost high-resolution robot touch," *IEEE Robotics and Automation Letters*, vol. 7, no. 4, pp. 9382–9388, 2022.

[23] L. Van Duong and V. A. Ho, "Large-scale vision-based tactile sensing for robot links: Design, modeling, and evaluation," *IEEE Transactions on Robotics*, vol. 37, no. 2, pp. 390–403, 2021.

[24] Q. K. Luu, N. H. Nguyen, and V. A. Ho, "Simulation, learning, and application of vision-based tactile sensing at large scale," *IEEE Transactions on Robotics*, vol. 39, no. 3, pp. 2003–2019, 2023.

[25] Q. K. Luu, D. Q. Nguyen, N. H. Nguyen, and V. A. Ho, "Soft robotic link with controllable transparency for vision-based tactile and proximity sensing," in *IEEE International Conference on Soft Robotics*, 2023, pp. 1–6.

[26] P. Svarny, J. Rozlivek, L. Rustler, M. Sramek, and et al., "Effect of active and passive protective soft skins on collision forces in human–robot collaboration," *Robotics and Computer-Integrated Manufacturing*, vol. 78, p. 102363, 2022.

[27] I. . Robotics, "Robots and robotic devices — collaborative robots," in *ISO/TS 15066:2016*, 2016.